Journal of the Serbian Chemical Society
JSCS-info@shd.org.rs • www.shd.org.rs/JSCS

ACCEPTED MANUSCRIPT

Please cite this article as S. Petković, J. Petrović, Đ. Janaćković, and R. Petrović, *J. Serb. Chem. Soc.* (2026) https://doi.org/10.2298/JSC260614045P

Journal of the Serbian Chemical Society
JSCS-info@shd.org.rs • www.shd.org.rs/JSCS
J. Serb. Chem. Soc. **00(0)** 1-14 (2026)
JSCS–14026
Original scientific paper
Published DD MM, 2026

Thermal copolymerization of urea with aromatic compounds to modify g-C_3N_4 for Cr(VI) removal

SOFIJA PETKOVIĆ[1]*, JANA PETROVIĆ[1], ĐORĐE JANAĆKOVIĆ[2] AND RADA PETROVIĆ[2]

[1]*Innovation Center of the Faculty of Technology and Metallurgy in Belgrade, Ltd, Belgrade, Serbia, and* [2]*University of Belgrade, Faculty of Technology and Metallurgy, Belgrade, Serbia.*

(Received 14 June; revised 14 July; accepted 6 August 2026)

Abstract: Graphitic carbon nitride (g-C_3N_4) has attracted considerable attention as a photocatalyst for the reduction of toxic Cr(VI) to less harmful Cr(III) due to its visible-light response, chemical stability, and low toxicity. However, its practical application is limited by the rapid recombination of photogenerated charge carriers. In this study, g-C_3N_4 was modified by thermal copolymerization of urea with two aromatic additives, 2-amino-5-nitrothiazole (ANT) and 1,5-dihydroxynaphthalene (DHN), using 10 or 50 mg of additive per 20 g of urea. The obtained materials were characterized by EDX, XRD, FTIR, FESEM, DRS, and PL spectroscopy. Photocatalytic Cr(VI) reduction was evaluated under simulated solar irradiation at pH 3.0 ± 0.1 in the presence of citric acid. Structural characterization confirmed preservation of the g-C_3N_4 framework after modification, while only minor changes in morphology and optical properties were observed. All modified samples were photocatalytically active, with the DHN-modified sample containing 50 mg additive showing the highest activity. The results indicate that ANT is difficult to incorporate into the g-C_3N_4 structure, whereas DHN modification reduces charge-carrier recombination and enhances photocatalytic performance.

Keywords: photocatalysis; water purification; donor-acceptor modification; 2-amino-5-nitrothiazole; 1,5-dihydroxynaphthalene.

INTRODUCTION

Heavy metal pollution has become a growing environmental concern due to rapid industrial development. Chromium is of particular interest because of its extensive industrial applications and frequent release into aquatic systems.[1] Among its two main oxidation states, Cr(VI) is highly toxic and carcinogenic, posing serious risks to ecosystems and human health.[2] Despite strict regulatory

* Corresponding author. E-mail: spetkovic@tmf.bg.ac.rs
https://doi.org/10.2298/JSC260614045P

limits for chromium in water, Cr(VI) contamination remains a persistent environmental issue.[3]

Various treatment methods, including adsorption, precipitation, ion exchange, and bioremediation, have been explored for Cr(VI) removal.[4–6] However, their practical application is often restricted by high costs, energy demands, secondary pollution, or limited efficiency. Photocatalytic reduction has emerged as a sustainable alternative, enabling the conversion of toxic Cr(VI) into the less harmful Cr(III) species using light energy under mild operating conditions.[7,8]

Graphitic carbon nitride (g-C_3N_4) is a promising metal-free semiconductor for Cr(VI) reduction under visible light owing to its suitable band structure and strong reduction potential.[9] However, the photocatalytic performance of pristine g-C_3N_4 is limited by several drawbacks, including the rapid recombination of photogenerated electron-hole pairs and relatively small specific surface area.[10] These limitations restrict charge separation and the availability of active sites, resulting in inefficient utilization of visible light and reduced photocatalytic activity under solar irradiation.

Various methods have been applied to modify g-C_3N_4 to overcome these limitations. Common approaches include formation of heterojunctions,[11] heteroatom doping,[12] and introduction of defects (carbon or nitrogen vacancies).[13] However, the weak bonding between heterojunction components contributes to low heterojunction stability and, more importantly, to potential secondary water pollution. On the other hand, doping and defect engineering may result in the introduction of new recombination sites, which can reduce the photocatalytic activity.[13]

Among the numerous strategies developed to improve the photocatalytic performance of g-C_3N_4, the construction of donor-acceptor (D-A) architectures has attracted considerable attention because of its ability to promote charge delocalization within π-conjugated systems.[14,15] Incorporation of π-conjugated aromatic moieties (benzene, furan, thiophen, *etc*.) into the carbon nitride framework generates electron-rich (donor) and electron-deficient (acceptor) units with different electron affinities.[16] The resulting internal electric field facilitates the separation of photogenerated charge carriers and enhances charge transfer. Furthermore, the electron affinity difference between donor and acceptor units promotes π-electron delocalization,[17] while π-π interactions within the D-A structure strengthen electronic coupling, thereby improving charge-carrier separation and migration.[18]

Aromatic co-monomers have emerged as an effective way of constructing such D-A architectures and tailoring the electronic structure of g-C_3N_4. Nitrogen-containing aromatic molecules based on pyridine[19] and pyrimidine[20] rings have been employed as co-monomers to construct D-A structures in g-C_3N_4, leading to enhanced charge transport and photocatalytic activity. This can be explained by

the fact that heteroatom aromatic rings (like pyridine and pyrimidine) are superior to benzene because the nitrogen atoms in the ring induce an electrostatic potential that leads to a redistribution of the Highest Occupied Molecular Orbital (HOMO) and Lowest Unoccupied Molecular Orbital (LUMO), resulting in spatial charge separation.[21] It was demonstrated that heteroaromatic building blocks provide a versatile platform for electronic structure engineering and performance enhancement of carbon nitride photocatalysts.[22]

Sulfur-containing aromatic compounds have shown considerable promise for enhancing photocatalytic activity. For example, the incorporation of 2-aminothiophene-3-carbonitrile into the g-C_3N_4 framework through thermal copolymerization with urea resulted in enhanced visible-light absorption, more efficient charge separation, and significantly improved photocatalytic performance.[23] These improvements were attributed to the successful incorporation of the thiophene unit, whose sulfur-containing π-conjugated structure modifies the electronic properties of carbon nitride and facilitates charge-carrier migration.

Despite these advances, thiazole-based aromatic modifiers remain largely unexplored. In particular, 2-amino-5-nitrothiazole (ANT) has not yet been investigated as a co-monomer for g-C_3N_4 synthesis, to the best of our knowledge. ANT is an especially attractive candidate because it combines sulfur and nitrogen heteroatoms within a single aromatic ring and contains both an electron-donating amino group and an electron-withdrawing nitro group. Such a molecular architecture is expected to strengthen donor-acceptor interactions, promote charge separation, and enhance visible-light absorption more effectively than previously reported heteroaromatic modifiers. Liang *et al*. reported that incorporating benzothiazole-2-carbaldehyde into the carbon nitride framework enhanced photocatalytic performance for both H_2O_2 production and RhB degradation.[24]

In addition to heteroaromatic compounds, bicyclic aromatic molecules represent another promising class of modifiers owing to their inherently extended π-conjugated systems.[25] Naphthalene-based structures provide a larger delocalization field than monocyclic aromatics, which can facilitate charge transport and suppress charge recombination.[26] Although naphthalene derivatives have previously been employed for donor-acceptor modification through a single anchoring group,[27] stronger electronic coupling with the carbon nitride framework may be achieved using molecules containing multiple reactive functionalities. In this regard, 1,5-dihydroxynaphthalene (DHN), bearing two hydroxyl groups capable of participating in condensation reactions, represents an attractive candidate for constructing more strongly integrated donor-acceptor architectures within the g-C_3N_4 framework.

This study investigated the possibility of enhancing the photocatalytic efficiency of g-C_3N_4 for the reduction of Cr(VI) in water by extending the π-

conjugated system by thermal copolymerization of urea and different quantities of either ANT or DHN. The photocatalysts were characterized using FESEM, EDX, XRD, DRS, FTIR and PL spectroscopy. The photocatalytic reduction of Cr(VI) was investigated under simulated solar irradiation at a constant pH.

EXPERIMENTAL

Pristine g-C_3N_4 was synthesized by thermal polymerization of urea (99.8%, VWR Chemicals) in a muffle furnace in an air atmosphere, at 550°C for 4 h in a covered crucible at a heating rate of 10°C/min. After cooling to room temperature, the obtained sample was ground into a fine powder and denoted as CN.

Modified g-C_3N_4 samples were prepared via thermal copolymerization of urea and aromatic additives. Briefly, 20 g of urea was thoroughly mixed with a predetermined amount (10 or 50 mg) of either ANT (2-amino-5-nitrothiazole, 97%, Sigma-Aldrich) or DHN (1,5-dihydroxy-naphthalene, Fluka AG, Buchs SG) using an agate mortar. The mixtures were then thermally treated under the same conditions as CN (550°C for 4 h in an air atmosphere, heating rate 10°C/min). Once cooled to room temperature, the samples obtained were ground in an agate mortar and labelled CN-xANT or CN-xDHN, where x represents the mass of the aromatic additive (mg) used in the synthesis.

An energy-dispersive X-ray (EDX) analysis was used for elemental analysis of the samples. EDX analysis was performed on an INCAx-act LN2-free analytical silicon drift detector of characteristic X-rays with PentaFET® Precision and Aztec 4.3 software package (Oxford Instruments) connected to a TESCAN Mira 3 MXU. All results obtained are presented as the arithmetic average of three measurements, expressed in weight percentages. The magnification used was 1000 x.

The morphology of the samples was determined using field emission scanning electron microscopy (FESEM, Tescan Mira 3 XMU) at a working voltage of 20 kV. Before analysis, the samples were coated with a thin layer of gold to ensure conductivity using a sputter coater (Polaron SC503, Fisons Instruments).

FTIR spectra were recorded using a Thermo Scientific Nicolet iS10 spectrometer. The measurements were performed in the wavenumber range of 400 to 4000 cm^{-1} operating in the attenuated total reflectance (ATR) technique, employing a resolution of 4 cm^{-1} and 20 scans per sample. The Omnic 9 software program was used for data collection and processing.

X-ray diffractograms were recorded using a Proto AXRD Benchtop diffractometer in Bragg-Brentano geometry with Cu Kα radiation (λ = 0.154 nm). Data were collected over the 2θ range 10-60° with a step size of 0.015° and a dwell time of 3 s per step.

Diffuse reflectance UV-Vis (DRS) spectra were collected using a Shimadzu UV-2600 spectrophotometer equipped with an ISR-2600 Plus integrating sphere and with $BaSO_4$ as the reflectance standard. Spectra were acquired over the 200-800 nm wavelength range. The reflectance data were transformed using the Kubelka-Munk function $F(R) = (1-R)^2/2R$, where R is the diffuse reflectance.[28]

The absorption edge wavelength (λ_g) was determined by extrapolating the linear portion of the absorption onset in the Kubelka-Munk plot to the baseline. Based on the λ_g, the value of the band gap energy (E_g) was calculated using the formula $E_g = 1240/\lambda_g$.[28]

Photoluminescence (PL) spectra were recorded on a Fluorolog-3 FL3-221 spectrofluorometer (Horiba Jobin-Yvon) using a 450 W Xenon lamp as the excitation source, with an excitation wavelength set at 370 nm.

Photocatalytic activity was evaluated based on the reduction of Cr(VI). A 10 mg/l Cr(VI) stock solution was prepared by dissolving $K_2Cr_2O_7$ (99.9%, Hemo) in deionized water and adjusting the pH to 3.0 ± 0.1 with 10 vol.% H_2SO_4 (96%, Lachema). For each experiment, 0.02 g of photocatalyst was dispersed in 40 ml of the Cr(VI) solution. Then, 0.133 ml of a 20 g/l citric acid solution (99.8%, Lachner) was added as a hole scavenger. The suspension was transferred to a water-jacketed reactor, where it was magnetically stirred and kept in the dark for 30 minutes. Preliminary experiments have shown that this is sufficient time to achieve adsorption-desorption equilibrium for all samples. Solar-simulating light (Osram Ultra-Vitalux 300 W lamp) was used for the experiments. The lamp-reactor distance and light intensity were held constant throughout the experiments. During illumination, 1 ml samples were withdrawn from the reactor every 15 minutes, filtered through a 0.22 μm PVDF syringe filter to remove catalyst particles, and then analyzed for Cr(VI) concentration. Cr(VI) concentrations were determined spectrophotometrically using a Shimadzu UV-1800 after complexation with 1,5-diphenylcarbazide (≥99%, Sigma-Aldrich). The resulting colored complex was monitored at its characteristic absorption maximum at 542 nm. A second photocatalytic cycle was performed using the sample which showed the best result, following the same procedure. Briefly, after photocatalytic reduction, the photocatalyst was separated by centrifugation (5 min at 6000 rpm), thoroughly washed twice with distilled water and once with ethanol (99.9%, Betahem). The washed photocatalyst was dried at 60°C overnight and reused in a fresh reaction solution under identical conditions.

RESULTS AND DISCUSSION

The elemental composition of the synthesized photocatalysts was analyzed by EDX and the results are given in Table I. According to the chemical formula of g-C_3N_4, the theoretical elemental composition is 60.86 wt.% N and 39.14 wt.% C. The compositions determined by EDX were generally consistent with these stoichiometric values. The CN-10ANT and CN-50ANT samples exhibit elemental compositions comparable to pristine CN, with only trace amounts of sulfur detected. In contrast, the DHN-modified samples show a small oxygen content, which may be associated with the oxygen-containing functional groups of the DHN additive. The relatively low concentration of additional elements detected by EDX is consistent with the small quantity of added modifiers, suggesting that the bulk elemental composition remains largely unchanged after modification.

TABLE I. Elemental composition of synthesized samples in wt. %

Photocatalyst	C	N	S	O
CN	33.6 ± 0.50	66.4 ± 0.50	--	--
CN-10ANT	32.7 ± 0.54	67.3 ± 0.54	0.01 ± 0.01	--
CN-50ANT	32.9 ± 0.41	67.1 ± 0.41	0.01 ± 0.03	--
CN-10DHN	32.8 ± 0.55	67.1 ± 0.59	--	1.59 ± 0.34
CN-50DHN	35.5 ± 0.37	62.6 ± 0.39	--	1.90 ± 0.22

However, the color of the samples (Fig. 1) indicates some structural modifications during synthesis. Pristine CN exhibited a pale yellow color, whereas the CN-xANT samples became progressively darker with increasing ANT content.

In contrast, CN-10DHN displayed a grayish-yellow color and CN-50DHN a dark gray color. Although EDX analysis does not provide evidence of substantial additive incorporation, the pronounced color changes suggest that the presence of ANT and DHN influenced the properties of the resulting materials.

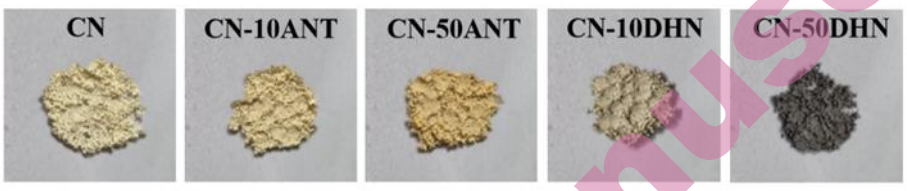

Fig. 1. Photographs of synthesized samples

The crystal structure of the synthesized photocatalysts was investigated using XRD, and the resulting diffractograms are presented in Fig. 2A. All samples exhibit the characteristic diffraction pattern of g-C_3N_4, confirming the successful formation of the g-C_3N_4 framework. Two characteristic diffraction peaks are observed at approximately 13° and 27°, corresponding to the (100) and (002) crystallographic planes of the hexagonal g-C_3N_4 phase (JCPDS No. 87-1526).[29] The weak reflection at around 13° is attributed to the in-plane structural ordering of heptazine units, whereas the intense peak near 27° originates from the interlayer stacking of conjugated aromatic layers within the graphitic structure.[14]

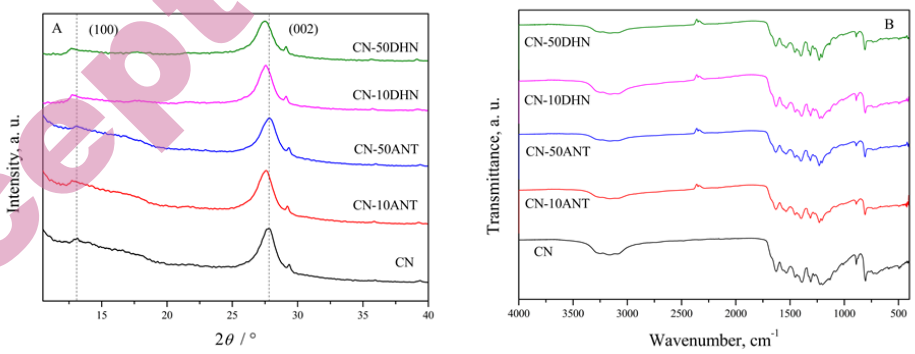

Fig. 2. XRD diffractograms (A) and FTIR spectra (B) of synthesized samples

Comparison of the XRD patterns reveals that the modification with ANT and DHN does not induce the formation of new crystalline phases. This indicates that the original g-C_3N_4 framework is maintained after modification. The position of the (002) reflection remains largely unchanged for CN-50ANT, while a slight shift toward lower 2θ values is observed for CN-10ANT, CN-10DHN, and CN-50DHN.

Such a shift suggests a slight increase in interlayer spacing, indicating a minor modification in layer stacking without altering the overall g-C_3N_4 structure.[30]

The intensity of the (002) diffraction peak is slightly lower for the 50-samples. The reduced peak intensity, particularly for CN-50DHN, suggests a decrease in the long-range stacking order of layers. However, no significant peak broadening is detected, suggesting that the overall layered structure remains essentially unchanged after modification.

The chemical structure of the synthesized photocatalysts was investigated using FTIR spectroscopy. As shown in Fig. 2B, the FTIR spectrum of pristine CN exhibits the characteristic vibrational features of g-C_3N_4, similar to previously reported data.[14] A broad absorption band in the range of 3000-3500 cm^{-1} is attributed to the stretching vibrations of N-H groups originating from free amino groups and O-H vibrations associated with adsorbed water molecules.[30] The band observed around 889 cm^{-1} can be attributed to the deformation vibration of N-H bonds, indicating the presence of incompletely condensed amino groups within the g-C_3N_4 structure. The intense absorption region between 1200 and 1650 cm^{-1} is assigned to the stretching vibrations of C-N and C=N bonds within the conjugated heptazine framework of g-C_3N_4.[14] The characteristic band at approximately 810 cm^{-1} corresponds to the breathing vibration of the tri-s-triazine units, confirming the formation of the polymeric carbon nitride structure.

The characteristic vibrational modes of ANT, including NH_2 stretching (3300-3500 cm^{-1}), NO_2 stretching (1320-1550 cm^{-1}), and C-S stretching vibrations (622-772 cm^{-1}), were not observed in the modified samples.[31,32] In particular, no distinct absorption attributable to C-S stretching was detected. The characteristic FTIR bands of DHN include O-H stretching (~3291 cm^{-1}), O-H deformation (~1371 cm^{-1}), C-OH stretching (~1257 cm^{-1}), and aromatic C-H deformation vibrations at 756 and 810 cm^{-1}.[33] The aforementioned features overlap with the broad N-H stretching and C-N/C=N stretching bands of g-C_3N_4. Consequently, the FTIR spectra of all modified samples closely resemble that of pristine CN, showing neither additional absorption bands nor significant peak shifts. Therefore, FTIR analysis does not provide evidence for the incorporation of ANT or DHN into the g-C_3N_4 framework and indicates that the chemical structure of g-C_3N_4 remains essentially unchanged after the modification procedure. However, it is possible that the analysis is not sensitive enough to detect changes, having in mind small quantities of modifiers.

A sharp feature around 2350 cm^{-1} observed in several spectra is attributed to atmospheric CO_2 present in the optical path during FTIR measurements and does not originate from the synthesized materials.[34]

The morphology of the synthesized photocatalysts was investigated by FESEM, and the results are shown in Fig. 3. The FESEM micrographs of pristine CN reveal the typical layered morphology of g-C_3N_4, consisting of irregularly stacked, sheet-like structures with folded edges.[35] The surface of pristine CN

exhibits a rough and heterogeneous texture. These structural features are commonly related to the release of gaseous species during the thermal condensation process, which can interfere with the close stacking of carbon nitride layers and contribute to the formation of a porous layered morphology.

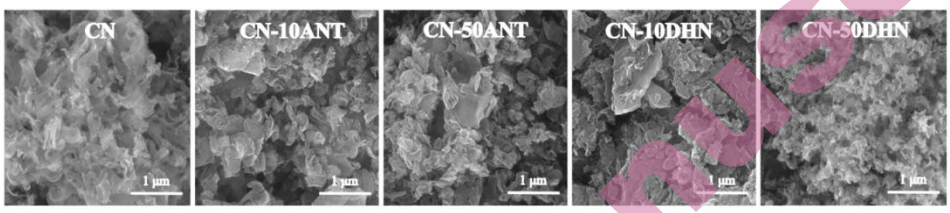

Fig. 3. FESEM micrographs of synthesized samples

The modified photocatalysts preserve the characteristic sheet-like morphology of pristine CN, indicating that the modification with ANT and DHN does not create significant morphological change. CN-10ANT, CN-50ANT, and CN-10DHN exhibit similar layered structures.

Among the obtained samples, CN-50DHN exhibits the most pronounced morphological changes compared to CN. Its surface is rougher, and its nanosheet structure contains more visible cavities. These characteristics point to the formation of a less compact and more flawed layered structure. During photocatalytic processes, these structural features may reveal surface locations and promote interfacial charge transfer.

The optical properties of the synthesized photocatalysts were investigated by DRS and PL analysis (Fig. 4). Fig. 4A shows the UV-Vis absorption spectra of the synthesized samples, with the corresponding λ_g and E_g values indicated on the plots.

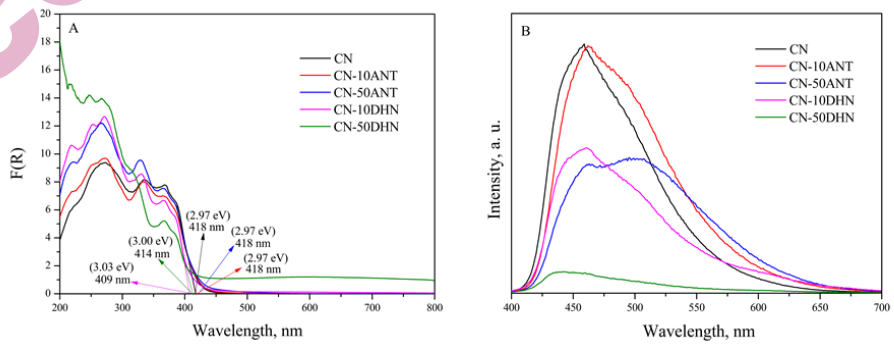

Fig. 4. UV-Vis absorption spectra of the synthesized samples (A), with the corresponding λ_g and E_g values (in parentheses) indicated, and PL spectra recorded under 370 nm excitation (B)

The UV-Vis diffuse reflectance spectra of all samples exhibit characteristic absorption features in the 200-400 nm region, commonly associated with electronic transitions within the conjugated heptazine framework of CN, namely π-π* transitions of the aromatic ring system and n-π* transitions involving the lone-pair electrons of nitrogen atoms.[36,37] For CN-10ANT, CN-50ANT, and CN-10DHN, the positions of these absorption features remain essentially unchanged compared with pristine CN, indicating that copolymerization at these loadings largely preserves the local electronic structure of the CN framework. In contrast, CN-50DHN exhibits noticeable differences in the absorption profile in the 200-400 nm region compared to the other samples. The band gap energy of pristine CN (Fig. 4A) is consistent with previously reported values for g-C_3N_4 synthesized from urea.[38] Such materials are known to exhibit slightly wider band gaps than g-C_3N_4 prepared from other commonly used precursors, such as melamine or dicyandiamide.[39]

The modified samples show only minor variations in the absorption edge, meaning that band gap energies remain within a narrow range. Obviously, the addition of ANT or DHN does not significantly modify the electronic band structure of CN.

In contrast to the other modified samples, CN-50DHN exhibits enhanced absorption across the entire visible-light region. Since the absorption edge remains essentially unchanged, the observed effect cannot be attributed to band-gap narrowing. The elevated absorption background is consistent with the grayish coloration of the sample and suggests the presence of DHN-derived species that act as additional visible-light absorbers. Consequently, the enhanced optical response of CN-50DHN is attributed to improved light harvesting in the visible region rather than to a modification of the intrinsic electronic structure of g-C_3N_4. Similar effects have been reported for naphthalene-modified g-C_3N_4 systems, where aromatic π-conjugated moieties act as sensitizers, extending visible-light absorption and promoting photocatalytic activity.[25,40] The enhanced absorption observed for CN-50DHN may therefore be associated with additional π-conjugated domains that facilitate photon capture and, potentially, charge-carrier separation and transport, while preserving the intrinsic band-gap transition of g-C_3N_4.

The pristine CN sample exhibited the most intense PL emission (Fig. 4B), whereas CN-10ANT displayed a comparable emission intensity, suggesting that the small quantities of ANT did not significantly alter the recombination behavior of photogenerated charge carriers. On the other hand, the reduced PL intensities observed for the remaining modified samples indicate enhanced charge separation and a lower recombination rate.[41] Among all samples, CN-50DHN showed the lowest PL emission intensity, implying the most effective inhibition of electron-hole recombination. Although CN-50ANT and CN-10DHN exhibited similar

overall PL intensities, the former displayed two separated emission bands, suggesting two distinct recombination pathways or charge trapping centers.

The photocatalytic performance of the synthesized samples was evaluated for the reduction of Cr(VI) in aqueous solution under simulated solar irradiation (Fig. 5). Citric acid was added to the solution as a hole scavenger to prevent re-oxidation of Cr(III). Photocatalytic efficiency was monitored by measuring the relative Cr(VI) concentration (C/C_0) over irradiation time t. Before irradiation (negative time values in the plots), the system was kept in the dark to establish adsorption-desorption equilibrium between the photocatalyst surface and Cr(VI) species.

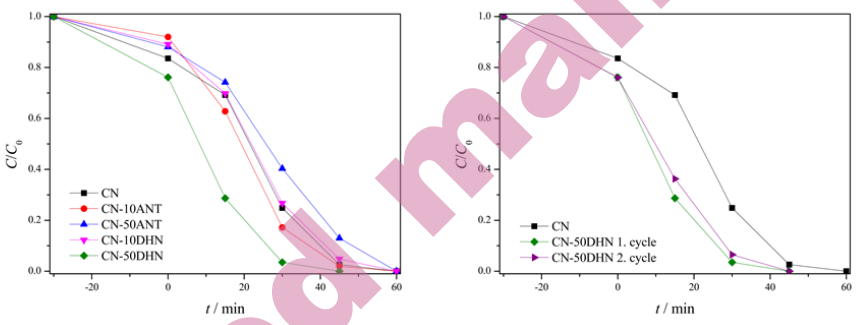

Fig. 5. Photocatalytic reduction of Cr(VI) (A) and repeated photocatalytic reduction of Cr(VI) for CN-50DHN sample (B)

Fig. 5A compares the Cr(VI) reduction behavior of CN, CN-10ANT, CN-50ANT, CN-10DHN, and CN-50DHN samples. Compared to pristine CN, CN-10ANT showed a slightly higher reduction rate, although the properties of that sample were practically the same as those of CN, especially band gap energy and recombination rate. On the other hand, CN-50ANT exhibited the lowest photocatalytic activity, suggesting that larger quantities of ANT have a negative effect on photocatalytic reduction. According to the PL spectra of the CN-50ANT sample (Fig. 4B), the appearance of two emission bands indicates the presence of two radiative recombination centers. The emission band at a lower wavelength is attributed to the intrinsic radiative recombination of g-C_3N_4, while the additional emission band at a higher wavelength suggests the formation of an additional recombination center after ANT incorporation. This additional center may originate from ANT-containing domains or surface-related electronic states.[42] Although XRD and FTIR analyses did not reveal the formation of a new crystalline phase or additional bonding features, the presence of a small amount of an amorphous ANT-derived phase cannot be excluded because of the low additive content. Photocatalytic efficiency of CN-10DHN was practically the same as that of CN, even though the recombination rate is lower, according to the PL intensity

(Fig. 4B). However, the band gap energy of CN-10DHN is higher than that of CN, indicating lower light absorption, which is probably the reason for the lower intensity of the PL peak. The CN-50DHN sample showed a faster reduction rate. Although CN-50DHN exhibited higher Cr(VI) adsorption during the dark period, the significantly faster decrease in Cr(VI) concentration under irradiation indicates that enhanced photocatalytic reduction, rather than adsorption alone, is responsible for its superior performance.

Because of its high activity, the reusability of CN-50DHN was tested in a second cycle (Fig. 5B). The recycled sample retained a similar Cr(VI) adsorption capacity, indicating that its properties were largely preserved. The subsequent photocatalytic reduction proceeded comparably to the fresh catalyst, achieving complete Cr(VI) removal within about 45 minutes. Although slightly higher Cr(VI) concentrations were observed during the irradiation period compared to the first cycle, the overall performance remained highly similar. These results demonstrate that CN-50DHN maintains its photocatalytic activity after reuse, indicating satisfactory short-term stability and retention of photocatalytic activity after reuse.

The superior performance of CN-50DHN can be correlated with the structural and photophysical characteristics identified in the characterization studies. XRD analysis revealed a lower stacking order and a slightly expanded interlayer spacing, while FESEM images showed increased surface heterogeneity. In addition, PL results demonstrated the lowest emission intensity among all samples, indicating the most efficient suppression of electron-hole recombination. This is likely due to the incorporation of a bicyclic aromatic moiety into the CN structure, which probably facilitates charge separation and transfer, leading to enhanced photocatalytic reduction of Cr(VI).

CONCLUSION

In this study, g-C_3N_4 was modified by thermal copolymerization of urea with different quantities of either DHN and ANT (10 or 50 mg on 20 g of urea) to evaluate the effect of aromatic additives on the photocatalytic reduction of Cr(VI). Characterization by EDX, XRD, FTIR, FESEM, DRS, and PL confirmed that the modification did not alter the fundamental structure of g-C_3N_4, although slight changes in layer stacking, morphology, and surface structure were observed, especially for the sample with 50 mg of DHN. The optical properties remained largely unchanged, indicating that the additives had little influence on the band gap energy.

The modified samples exhibited different charge carrier recombination behavior compared to g-C_3N_4, as shown by PL analysis. Among the investigated photocatalysts, the sample with 50 mg of DHN showed the lowest PL intensity, indicating the most efficient charge separation. This sample also exhibited the

highest photocatalytic activity toward Cr(VI) reduction under simulated solar irradiation and maintained its activity after the first cycle.

Overall, the results indicate that ANT is difficult to copolymerize with urea, while polymerization with DHN caused changes in the structural and photophysical properties of g-C_3N_4, probably due to the introduction of a bicyclic aromatic moiety into the g-C_3N_4 structure, leading to improved photocatalytic performance.

Acknowledgements: The authors wish to acknowledge funding from the Ministry of Science, Technological Development and Innovation of the Republic of Serbia through project contracts No. 451-03-34/2026-03/200135 and 451-03-33/2026-03/200287.

И З В О Д

ТЕРМАЛНА КОПОЛИМЕРИЗАЦИЈА УРЕЕ СА АРОМАТИЧНИМ ЈЕДИЊЕЊИМА ЗА МОДИФИКАЦИЈУ g-C_3N_4 У ЦИЉУ УКЛАЊАЊА Cr(VI)

СОФИЈА ПЕТКОВИЋ[1], ЈАНА ПЕТРОВИЋ[1], ЂОРЂЕ ЈАНАЋКОВИЋ[2], РАДА ПЕТРОВИЋ[2]

[1]Иновациони центар Технолошко-металуршког факултета у Београду д.о.о., Београд, Србија, и [2]Универзитет у Београду, Технолошко-металуршки факултет, Београд, Србија.

Графитни угљеник(IV)-нитрид (g-C_3N_4) привукао је значајну пажњу као фотокатализатор за редукцију токсичног Cr(VI) у мање штетан Cr(III) захваљујући активности под видљивом светлошћу, хемијској стабилности и ниској токсичности. Међутим, његову практичну примену ограничава брза рекомбинација фотогенерисаних носилаца наелектрисања. У овом раду, синтетисан је модификовани g-C_3N_4 термичком кополимеризацијом уреe са два ароматична једињења, 2-амино-5-нитротиазолом (ANT) и 1,5-дихидроксинафталеном (DHN), при чему је на 20 g уреe додато 10 или 50 mg једињења. Добијени материјали окарактерисани су применом EDX, XRD, FTIR, FESEM, DRS и PL спектроскопије. Фотокаталитичка редукција Cr(VI) испитивана је под симулираним сунчевим зрачењем при pH 3,0 ± 0,1 у присуству лимунске киселине као хватача шупљина. Резултати карактеризација потврдили су очување структуре g-C_3N_4 након модификације, док су уочене само мање промене у морфологији и оптичким својствима. Сви модификовани узорци показали су фотокаталитичку активност у редукцији Cr(VI), при чему је узорак модификован са 50 mg DHN показао највећу активност. Резултати указују да се ANT тешко уграђује у структуру g-C_3N_4, док модификација са DHN смањује рекомбинацију носилаца наелектрисања и побољшава фотокаталитичке перформансе.

(Примљено 14. јуна; ревидирано 14. јула; прихваћено 6. августа 2026.)

REFERENCES

1. Md. Nur-E-Alam, Md. A. S. Mia, F. Ahmad, Md. M. Rahman, *Appl. Water Sci.* **10** (2020) 205 (https://doi.org/10.1007/s13201-020-01286-0)
2. H. Hossini, B. Shafie, A. D. Niri, M. Nazari, A. J. Esfahlan, M. Ahmadpour, Z. Nazmara, M. Ahmadimanesh, P. Makhdoumi, N. Mirzaei, E. Hoseinzadeh, *Environ. Sci. Pollut. Res.* **29** (2022) 70686–70705 (https://doi.org/10.1007/s11356-022-22705-6)

3. World Health Organization, *Chromium in Drinking-Water: Background Document for Development of WHO Guidelines for Drinking-Water Quality*, World Health Organization, Geneva, 2020
4. C. E. Barrera-Díaz, V. Lugo-Lugo, B. Bilyeu, *J. Hazard. Mater.* **223–224** (2012) 1–12 (https://doi.org/10.1016/j.jhazmat.2012.04.054)
5. Y. Xing, Y. Zheng, X. Wang, *Environ. Adv.* **19** (2025) 100614 (https://doi.org/10.1016/j.envadv.2025.100614)
6. H. Peng, J. Guo, *Environ. Chem. Lett.* **18** (2020) 2055–2068 (https://doi.org/10.1007/s10311-020-01058-x)
7. A. Saravanan, P. S. Kumar, D.-V. N. Vo, P. R. Yaashikaa, S. Karishma, S. Jeevanantham, B. Gayathri, V. D. Bharathi, *Environ. Chem. Lett.* **19** (2021) 441–463 (https://doi.org/10.1007/s10311-020-01077-8)
8. W. Zeng, Y. Luo, C. Wang, Z. Liu, M. Xue, X. Xie, *Environ. Pollut. Bioavailab.* **37** (2025) 2493057 (https://doi.org/10.1080/26395940.2025.2493057)
9. X. Wang, L. Li, J. Meng, P. Xia, Y. Yang, Y. Guo, *Appl. Surf. Sci.* **506** (2020) 144181 (https://doi.org/10.1016/j.apsusc.2019.144181)
10. D. S. Pattanayak, D. Pal, J. Mishra, C. Thakur, *Environ. Sci. Pollut. Res.* **30** (2023) 25546–25558 (https://doi.org/10.1007/s11356-022-20170-9)
11. M. G. Sahini, A. Parmain, I. Onoka, S. F. Mwanga, *J. Alloys Compd.* **1044** (2025) 183642 (https://doi.org/10.1016/j.jallcom.2025.183642)
12. H. Moradi, M. Haghighi, G. Foroutan, M. Shabani, *Mater. Sci. Semicond. Process.* **206** (2026) 110398 (https://doi.org/10.1016/j.mssp.2025.110398)
13. M. I. Nabeel, T. Gulzar, S. Kiran, N. Ahmad, S. A. Raza, U. Batool, Z. A. Rehan, *Int. J. Energy Res.* **2025** (2025) 5599894 (https://doi.org/10.1155/er/5599894)
14. H. Che, C. Liu, G. Che, G. Liao, H. Dong, C. Li, N. Song, C. Li, *Nano Energy* **67** (2020) 104273 (https://doi.org/10.1016/j.nanoen.2019.104273)
15. J. Liu, R. Zou, H. Zhang, Y. Song, Y. Liu, S. Yang, R. Xia, E. I. Iwuoha, U. Feleni, S. Admassie, X. Peng, *Appl. Catal. B Environ.* **357** (2024) (https://doi.org/10.1016/j.apcatb.2024.124312)
16. C. Zhang, Z. Ouyang, Y. Yang, X. Long, L. Qin, W. Wang, Y. Zhou, D. Qin, F. Qin, C. Lai, *Chem. Eng. J.* **448** (2022) 137370 (https://doi.org/10.1016/j.cej.2022.137370)
17. X.-X. Wang, C.-R. Zhang, R.-X. Bi, Z.-H. Peng, A.-M. Song, R. Zhang, H.-X. He, J.-X. Qi, J.-W. Gong, C.-P. Niu, R.-P. Liang, J.-D. Qiu, *Adv. Funct. Mater.* **35** (2025) 2421623 (https://doi.org/10.1002/adfm.202421623)
18. N. Liu, J. Jiang, Z. Chen, B. Wu, S. Zhang, Y.-Q. Zhang, P. Cheng, W. Shi, *Angew. Chem. Int. Ed.* **62** (2023) e202312306 (https://doi.org/10.1002/anie.202312306)
19. C. Li, H. Wu, D. Zhu, T. Zhou, M. Yan, G. Chen, J. Sun, G. Dai, F. Ge, H. Dong, *Appl. Catal. B Environ.* **297** (2021) 120433 (https://doi.org/10.1016/j.apcatb.2021.120433)
20. Y. Liu, W. Miao, Z. Chen, D. Yao, J. Wang, X. Chen, S. Mao, *Chem. Eng. J.* **496** (2024) 153871 (https://doi.org/10.1016/j.cej.2024.153871)
21. Z. Ma, X. Zong, Q. Hong, L. Niu, T. Yang, W. Jiang, D. Qu, L. An, X. Wang, Z. Kang, Z. Sun, *Appl. Catal. B Environ.* **319** (2022) 121922 (https://doi.org/10.1016/j.apcatb.2022.121922)
22. Y. Zhu, B. Yang, X. Tian, J. Xiang, Z. Xie, Z. Le, *Res. Chem. Intermed.* **52** (2026) 3873–3891 (https://doi.org/10.1007/s11164-026-05986-1)
23. M. Zhang, X. Wang, *Energy Env. Sci* **7** (2014) 1902–1906 (https://doi.org/10.1039/C3EE44189J)

24. H. Liang, Q. Xu, R. Cheng, S. Jing, F. Chen, P. Tsiakaras, *Carbon* **244** (2025) 120603 (https://doi.org/10.1016/j.carbon.2025.120603)
25. Q. Zhang, J. Chen, H. Che, P. Wang, B. Liu, Y. Ao, *ACS Mater. Lett.* **4** (2022) 2166–2186 (https://doi.org/10.1021/acsmaterialslett.2c00604)
26. Y. Xu, T. Yan, N. Chen, H. Chen, A. Xue, X. Zhang, *Int. J. Hydrog. Energy* **51** (2024) 1417–1428 (https://doi.org/10.1016/j.ijhydene.2023.07.296)
27. K. Li, M. Sun, W.-D. Zhang, *Carbon* **134** (2018) 134–144 (https://doi.org/10.1016/j.carbon.2018.03.089)
28. C. Yu, K. Yang, Q. Shu, J. C. Yu, F. Cao, X. Li, X. Zhou, *Sci. China Chem.* **55** (2012) 1802–1810 (https://doi.org/10.1007/s11426-012-4721-8)
29. M. Devi, J. Shikhar, S. Sharma, *J Mater Chem A* **13** (2025) 42343–42354 (https://doi.org/10.1039/D5TA06469D)
30. S. Song, C. Lu, X. Wu, S. Jiang, C. Sun, Z. Le, *Appl. Catal. B Environ.* **227** (2018) 145–152 (https://doi.org/10.1016/j.apcatb.2018.01.014)
31. J. Bahadur, S. Cho, P. Pandey, S. Yoon, D.-G. Lee, J. Ryu, J. T. Song, J. Lim, D.-W. Kang, *Sol. RRL* **8** (2024) 2300912 (https://doi.org/10.1002/solr.202300912)
32. Vinodkumar, J. Keshavayya, I. Pushpavathi, C. T. Keerthikumar, M. R. Maliyappa, B. N. Ravi, *Struct. Chem.* **31** (2020) 1317–1329 (https://doi.org/10.1007/s11224-020-01493-0)
33. B. Lu, L. Zeng, J. Xu, Z. Le, H. Rao, *Eur. Polym. J.* **45** (2009) 2279–2287 (https://doi.org/10.1016/j.eurpolymj.2009.05.005)
34. B. C. Smith, *Fundamentals of Fourier Transform Infrared Spectroscopy*, 2nd ed CRC Press, Boca Raton, Florida, 2011
35. S. Fazli-Shokouhi, F. Nasirpouri, B. Ramezanzadeh, *J. Mater. Res. Technol.* **38** (2025) 5554–5578 (https://doi.org/10.1016/j.jmrt.2025.08.287)
36. A. Lewalska-Graczyk, P. Pieta, G. Garbarino, G. Busca, M. Holdynski, G. Kalisz, A. Sroka-Bartnicka, R. Nowakowski, M. Naushad, M. B. Gawande, R. Zbořil, I. S. Pieta, *ACS Sustain. Chem. Eng.* **8** (2020) 7244–7255 (https://doi.org/10.1021/acssuschemeng.0c02267)
37. M. M. Hasan, M. S. Hossain, M. D. Islam, M. M. Rahman, A. S. Ratna, S. Mukhopadhyay, *ACS Appl. Mater. Interfaces* **15** (2023)(https://doi.org/10.1021/acsami.3c05659)
38. Y. Shao, C. Liu, H. Ma, J. Chen, C. Dong, D. Wang, Z. Mao, *Chem. Phys. Lett.* **801** (2022) 139748 (https://doi.org/10.1016/j.cplett.2022.139748)
39. L. Ma, Z. Li, Z. Jiang, X. Wu, S. Chang, S. A. C. Carabineiro, K. Lv, *Chin. J. Struct. Chem.* **43** (2024) 100416 (https://doi.org/10.1016/j.cjsc.2024.100416)
40. M. Cao, Y. Qiu, M. Yang, Y. Zhang, Q. Li, S. Zhang, P. Li, Q. Sui, *Int. J. Hydrog. Energy* **97** (2025) 227–235 (https://doi.org/10.1016/J.IJHYDENE.2024.11.439)
41. L. Yang, J. Huang, L. Shi, L. Cao, Q. Yu, Y. Jie, J. Fei, H. Ouyang, J. Ye, *Appl. Catal. B Environ.* **204** (2017) 335–345 (https://doi.org/10.1016/j.apcatb.2016.11.047)
42. D. Das, D. Banerjee, D. Pahari, U. K. Ghorai, S. Sarkar, N. S. Das, K. K. Chattopadhyay, *J. Lumin.* **185** (2017) 155–165 (https://doi.org/10.1016/j.jlumin.2017.01.007)